Romanian Reports in Physics, Vol. 63, No. 1, P. 86–94, 2011

SEM INVESTIGATIONS OF CR-39 AND MICA-MUSCOVITE SOLID STATE NUCLEAR TRACK DETECTORS

C. COSTEA[1], O.G. DULIU[2], A. DANIS[3], S. SZOBOTKA[4]

[1] Geological Institute of Romania, 1 Caransebes Street, 012271 Bucharest, Romania
E-mail: *titicostea@yahoo.com*
[2]University of Bucharest, Department of Atomic and Nuclear Physics, P. O. Box MG-11, 7125 Magurele (Ilfov), Romania, E-mail: *duliu@b.astral.ro*
[3]National Institute for Nuclear Physics and Engineering, P.O.Box MG-6, 077125 Bucharest-Magurele, Romania
[4]National Institute for Marine Geology and Marine Geo-Ecology, 23-25, Dimitrie Onciul Street, 024053, Bucharest, Romania, E-mail: *szobi@usa.net*

Received Ianuary 5, 2010

Abstract. Scanning Electron Microscopy (SEM) was used in four different variants to investigate the trace distribution of alpha particles on an allyl diglycol carbonate (ADC) CR-39 as well as the fission fragments on a mica muscovite solid state nuclear trace detectors (SSNTD). Both were used to determine the absolute age of the manganese nodules. All images reveled with clarity the characteristic circular shape of cellulose acetate traces as well as the typical parallelogram-like traces of mica muscovite detectors. Corresponding image histograms were used to select the best SEM images acquisition variant. Consequently, in the case of ADC detector the secondary electrons image showed the best contrast, while in the case of the mica detector the secondary electrons, both back scattered topographic and combined images presented a comparable contrast. This finding recommends SEM as an appropriate method to be used in conjunction with SSNTD investigation of the absolute geochronology of polymetallic nodules.

Key words: SEM, tracks detectors, CR-39, muscovite, geochronology, polymetallic nodules, image analysis.

1. INTRODUCTION

Since their first use in the measure of the neutron fluxes [1], solid-state nuclear track detectors (SSNTDs) have found a large field of applications in various domains of science such as nuclear physics [2], geochemistry [3–5] or geochronology [6–9].

With respect to other types of detectors currently used in nuclear physics to investigate charged radiation, SSTDs present a lot of advantages such as a significant low cost as well as simplicity in exploitation. This represents a remarkable ability to be used in various geometries and sizes: an integrating nature

that allows events to accumulate over a long interval of time as well as a differential sensitivity to charged particles such as alpha radiation or fission fragments, making them very popular among scholars.

Although traces made visible after etching are mainly investigated by using normal or confocal microscopes [6, 10, 11], scanning electron microscopy (SEM) irrespective of its some inherent difficulties regarding sample preparation is able to offer, due to its significant higher spatial resolution, a more detailed information concerning trace shape, trace volume, and trace orientations [12–14].

The existing SSNTDs, by their diverse nature can be used to detect almost all types of heavy charged radiation: protons, alpha particles of fission fragments as in the case of plastic detectors, and only fission fragments as in the case of inorganic detectors such as biotite or muscovite micas, apatite, sphene, zircon, volcanic glass, etc. [6, 8]. For this reason, both plastic and inorganic SSTDs were used successfully among others in mapping the distribution of thorium and uranium isotopes over the entire sections for a precise absolute geochronology as in the case of manganese nodules [15–19].

In the present work we report our result concerning tracks properties as revealed by SEM on two types of SSNTDs, *i.e*. allyl diglycole carbonate (ADC) CR-39 and mica muscovite; both used to investigate the distribution of ^{230}Th and respectively ^{231}Pa and other fissionable elements in a vertical section through a polymetallic nodule collected from the North Pacific Clarion-Clipperton abyssal plain. In performing this study, our aim was to determine the best conditions necessary for a complete and, as possible as, error free determination of trace density on the surface of both type of detectors.

2. MATERIALS AND METHODS

2.1. Samples

The investigated nodules with a discoid shape (7.6 by 5.3 cm) were dredged during the 1984 cruise of the Academic Aleksandr Karpinski research vessel in the Clarion-Clipperton region of the North Pacific Region (12-13°N and 137-138°W). Morphologically, this was a typical nodule for this province, but due to the collecting method its in situ orientation has been indirectly obtained by taking into consideration details such as growth asymmetry and surface texture [20].

For further investigations concerning the radial distribution of ^{238}U, ^{231}Pa, and ^{230}Th the nodule was embedded in acrylic resin following a procedure commonly used in soil science and transversally sectioned in slices of about 2.5 mm in thickness. After that, the same vertical section was investigated twice: once by keeping it in full contact with a ADC CR-39 foil for six months to register the alpha particles and a second time by placing the same section in tight contact with two mica muscovite foils to record the fission fragments and by

irradiating them for 2 hours at a total neutron fluency of 8.5 10^{15}n/cm^2 in the VVR –S type nuclear reactor at the National Institute of Physics and Nuclear Engineering - Horia Hulubei.

2.2. Detectors

We have chosen for our study the ADC CR-39 (Page, England) for its sensitivity to alpha particles [19] and the mica muscovite for its specific ability to detect only fission fragments [21].

In the case of plastic detector CR-39 the tracks were evidenced by etching it for 18 days in a 30 % KOH aqueous solution at the room temperature while the fission-tracks were developed by keeping the muscovite foils in a 40 % HF solution for 2.5 h. In both cases, after etching the detector foils were rinsed abundantly in distilled water and dried.

To be investigated by SEM, both detectors were cleaned by immersing them in an ultrasound bath for 5 minutes, washed with ethylic alcohol and dried. Subsequently, during the process of vacuum evaporation they were initially covered with graphite and later on with a thin (~ 0.05 μm) layer of silver and respectively copper. This was achieved by keeping samples in a vacuum evaporator to avoid any heat damage for about 2 minutes.

2.3. SEM AND IMAGE ANALYSIS

SEM investigations were performed by using a REM-100U microscope provided with a digital acquisition unit for both imaging and spectrometric data. In imaging mode, the instrument can supply four different images of the same surface, *i.e.* secondary electrons (SEI), back scattered electrons (COMPO), absorbed electrons (ABS) as well as topography mode (TOPO) at magnifications varying between 40 and 150 000. In this mode, the maximum investigated area of 3×3 mm corresponds to minimum magnification, but by increasing the distance between electron gun and sample, the maximum area can be increased up to 8.5×8.5 mm. For elemental analysis, both wave dispersive (WDX) and energy dispersive (EDAX) modes are used. Regarding EDAX it is worth mentioning that the instrument generates maps depicting the distribution of individual elements over investigated surface. At an acceleration potential of 30 kV, the best spatial resolution attained was of 5 nm.

All electronic images supplied by REM-100U digital acquisition system were subsequently analyzed by using the freeware Image J [22] image processing programs. Therefore, in order to determine the most suitable procedure to examine the tracks distribution we have scanned the same section by using all four modes: SE, TOPO, COMPO as well as ABSORBED.

As all four images were obtained at the same magnification and with the same spatial resolution, we have chosen image contrast as discriminating criterion and half width of image histograms to quantify it. Accordingly, image histogram full width at half maximum (FWHM) seems to the best descriptor for image contrast, such that the narrower image histogram, the higher contrast was achieved.

3. RESULTS AND DISCUSSION

3.1. CR-39

To illustrate both SEM image quality and alpha tracks distribution, in Fig. 1 we have reproduced a low magnification secondary electrons SEM picture on the left-lower corner of a CR-39 detector after exposure, etching, and Cu covering. On this image which represents a section of 8.5×5.3 mm of the entire plate, typical almost circular alpha tracks are distinct and their distribution is marked with clarity on the inferior part of the picture of the nodule margin. It should be noticed that the lateral tracks are slightly deformed, due to spherical aberration. Despite this fact, because the trace density is more important for nodule geochronology, this irregularity is of a lesser importance in our case. Since the microscope vacuum chamber can house 10 times greater samples and their complete scan needs about half hour, it means that an entire detector measuring 8.5×6 cm can be entirely examined in detail concerning the local distribution of alpha tracks in about two working days. The only disadvantage with respect to optical microscopy consists of the need to cut the detector plate in more fragments to be separately scanned.

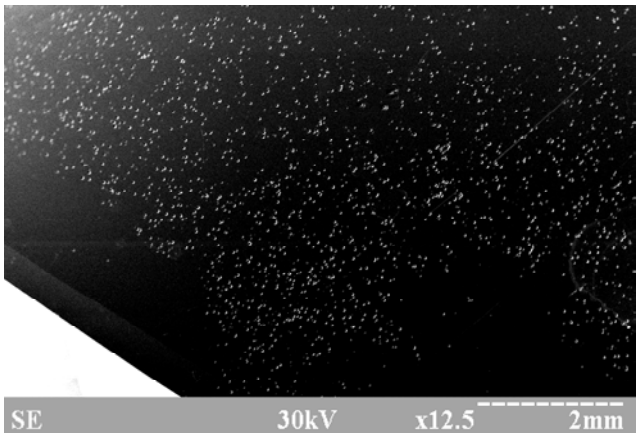

Fig. 1 – A low magnification (×12.5) SEM images of a fragment of about 8.5×5.3 mm of a CR-39 detector impressed by the alpha particles emitted mainly by 230Th and its descendents contained in a vertical section of a polymetallic nodule. The absence of tracks on the inferior part of image marks nodule boundary.

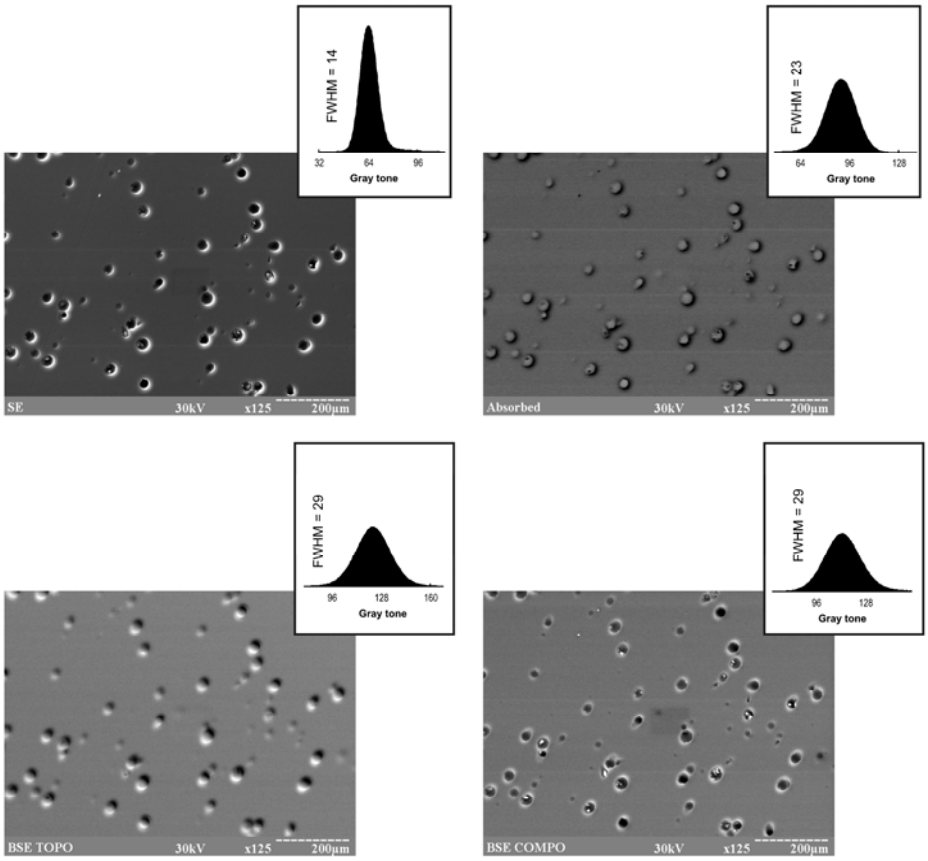

Fig. 2 – Four different SEM pictures of the same fragment of a CR-39 detector as well as corresponding image histograms (insets). Since narrower histograms characterized small FWHM correspond to contrast images, from this point of view, secondary electrons image seems to be more adequate for trace counting.

Since an image histogram depicts the distribution of gray tones, by means of ImageJ program we have generated the corresponding image histograms (Fig. 2, insets). As expected, all histograms presented a single peak whose FWHM (expressed in number of gray half-tones whose maximum number is 256) varied between 14 and 29, with the minimum values corresponding to SEI image (Fig. 2). It follows that, in accordance with above mentioned criterion, SE image seems to be the most adequate for further trace counting. The same images were used to determine the sizes alpha ray traces, whose average size was of 30.9 ± 4.8 μm while the TOPO mode images gave for the average trace depths a value of 3.5 ± 0.3μm.

Concerning the other images it is worth mentioning that the TOPO image is very similar to replica images reported in Ref. [12].

3.2. Mica detectors

For a better comparison between the two types of detectors, Fig. 3 illustrates a low magnification SE image of the mica detector which was processed in a similar manner as the cellulose one but finally vacuum covered by silver only. As in the precedent case, the SEM image shows with clarity not only the trace distribution but also some macroscopic defects that appeared on the mica surface due to an incipient cleavage (mica muscovite presents a perfect cleavage surface normal to b crystalline axis) which did not disturb the trace distribution.

To choose which techniques generate better images, we have investigated the same area at a higher magnification by means of the same four procedures, *i.e.* SE, TOPO, COMPO, and ABSORBED. Image J was also used to generate corresponding image histograms which in this case showed that except for TOPO, all other images presented a similar contrast. In our opinion, the observed differences between the image contrast in the case of cellulose and mica detectors can be explained by the detectors different nature. CR-39 presents a significant lower mechanical resistance to both radiation damage and chemical treatment. However, irrespective of these small differences, both types of detectors showed a remarkable resilience to all preliminary treatments necessary for a SEM examination, including vacuum metal plating.

Concerning mica detectors, it must be noticed that typical parallelogram-like (18,0 ± 1.6 μm × 11.6 ±1.5 μm) traces reflect the orientation of the crystalline axes *a* and *c*, a common trait to the majority of monoclinic minerals. Again TOPO mode allowed us to estimate the average depth of fission fragment traces to 0.17 ± 0.07 μm.

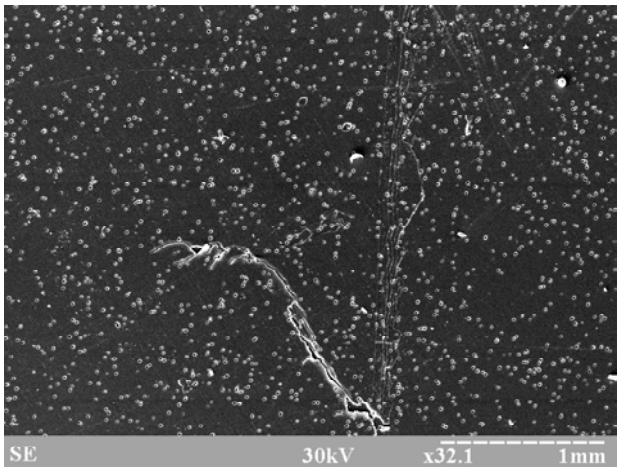

Fig. 3 – SEM image of a fragment of muscovite detector of about 3.8×2.6 mm impressed by the fission fragments emitted mainly by ^{231}Pa and U isotopes existing in the same vertical section of the polymetallic nodule as in Fig. 1.

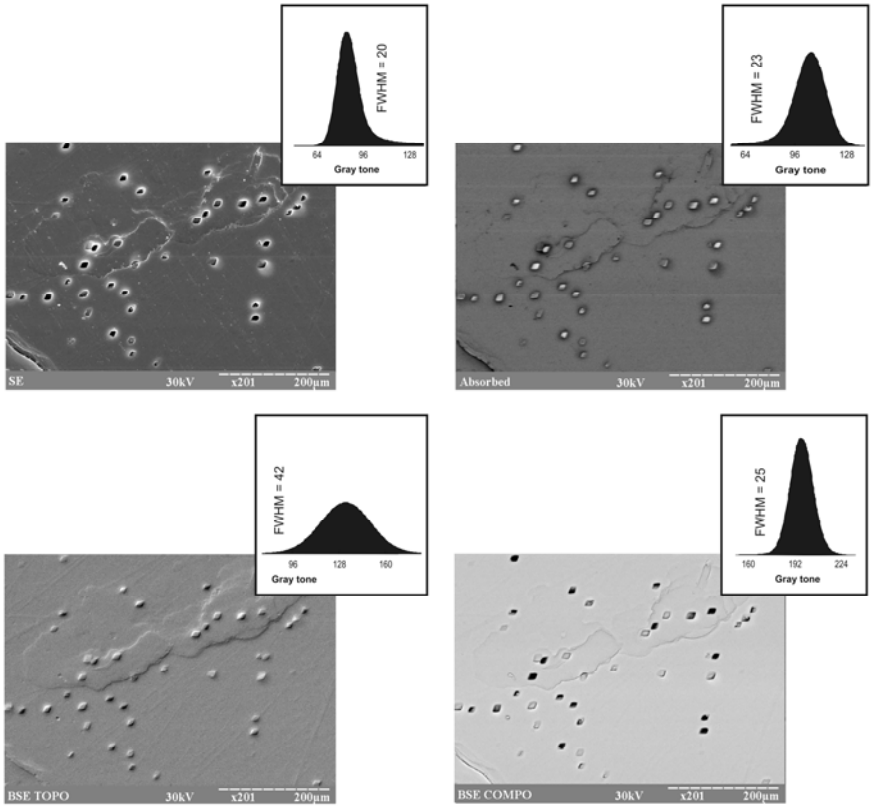

Fig. 4 – Four different SEM images of the same area of mica detector together with corresponding image histograms. In this case, at last three images, *i.e.* secondary electrons, topographic, and backscattered electrons have almost the same contrast characterized by almost equal values of FWHM, recommending them for further trace counting.

By comparing the SEM images recorded by cellulose and mica detectors with those previously reported by optical microscopy, SEM images seems to be of a better quality. By revealing with accuracy and lesser artifacts the traces contours, SEM is recommended as one of the most appropriate technique for SSNTDs investigation.

3. CONCLUDING REMARKS

SEM was used to investigate the traces shape and distribution on two different types of solid state nuclear tracks detectors (SSNTD), *i.e.* CR-39 allyl digycole carbonate and mica muscovite. Both SSNTDs were used to evidence the local distribution of ^{230}Th as well as fissile elements ^{213}Pa in a section of a polymetallic nodule with the final aim to establish its absolute geochronology.

Accordingly, on both types of detectors, it was possible to evidence with clarity the distribution of two different kinds of traces: the round ones characteristic for alpha ray on allyl digycole carbonate and the parallelogram-shape ones, typical for muscovite fission fragments detectors. In order to get the best images, four different SEM techniques were used, *i.e.* secondary electrons, topography, back scattered electrons, and absorption electrons.

As discriminating criterion we have used the full width at half maximum (FWHM) of the corresponding image histograms. Since we have used native, non processed SEM images, in the case of cellulose detector the secondary electrons image showed the best contrast, while in the case of mica detector, secondary electrons, topography, and back scattered electrons images showed to be of a similar quality.

By taking into account that all SEM images were almost free of artifacts and presented a better contrast than the optical ones despite the need for a preliminary vacuum metallization, SEM appears to be a very suitable method to be used in both alpha and fission tracks absolute geochronology.

Acknowledgments. We express our gratitude to Carolina Stamu-O'Brien for here help in revising the manuscript.

REFERENCES

1. R.L. Fleischer, P.B. Price, R.M. Walker, Nucl. Sci. Engin., **22**, 153–156 (1965).
2. R.L. Fleischer, P.B. Price, R.M. Walker, *Nuclear Tracks in Solids: Principles and Applications*, University of California Press, Berkeley, 1975.
3. C.P. Dewolf, C.J. Zeissler, A.N. Halliday, K. Mezger, E.J. Essene, *Geochim. Cosmochim*, Acta, **60**, 121-134 (1986).
4. S. Singh, B. Singh, A.S. Sandhu, G. Singh, Rad. Meas., **31**, 687–690 (1999).
5. G.R. Choppin, J.O. Liljenzin, J. Rydberg, *Radiochemistry and Nuclear Chemistry*, Butterworth-Heinemann, Oxford, 2001.
6. S.A. Durrani, R.K., *Bull. Solid State Nuclear Track Detection: Principles*, Methods and Applications, Pergamon Press, 1987.
7. M.A. Geyh, H. Schleicher, *Absolute Age Determination*, Springer, Berlin, 1990.
8. A. Dickin, *Radiogenic Isotope Geochemistry*, Cambridge University Press, 1995.
9. P. van den Haute, F. De Corte (Eds.) *Advances in Fission-Track Geochronology*, Kluwer Academic, Dordrecht, 1998.
10. F. Vaginay, M. Fromm, D. Pusset, G. Meesen, A. Chambaudet, A. Poffijin, Rad. Measur., **34**, 123–127 (2001).
11. A. Mostofizadeh, X. Sun, M.R. Kardan, J. Appl. Sci., **7**, 2261-2271 (2007).
12. K.N. Yu, F.M.F. Ng, J.P.Y. Ho, C.W.Y. Yip, D. Nikezic, Rad. Prot. Dosim., **111**, 93–96 (2004).
13. B. Sartowska, A. Szydłowski, M. Jaskóła, A. Korman, Rad. Measur., **40**, 347–350 (2005).
14. G.S. Sekhon, S. Kumar, C. Kaur, N.K. Verma, S.K. Chakarvarti, Rad. Measur., **43**, 1357–1359 (2008).
15. D. Heye, Prog. Oceanog., **7**, 163-239 (1978).

16. M.E. Andersen, J.D., MacDougall, Geophys. Res. Let., **4**, 351–353 (1977).
17. J.D. MacDougall, *The distribution of total alpha radioactivity in selected manganese nodules from the North Pacific: implications for growth processes*, in: J.L. Bischoff, D.Z. Piper (Editors), *Marine geology, oceanography of the Pacific manganese nodules province*, Plenum Publishing Corporation, New York, 1979 pp. 775–789.
18. I.E. Vlasova, Rad. Measur., **22**, 831–834 (1993).
19. I.E. Vlasova, Rad. Measur., **25**, 503–506 (1995).
20. W.J. Raab, M.A. Meylan, *Morphology*, in: G.P. Glasby (Editor), *Marine manganese deposits*, Elsevier, Amsterdam, 1977 pp. 109–146.
21. A. Danis, M. Oncescu, Nucl. Instr. Meth., **173**, 143–146 (1980)
22. ImageJ, http://rsbweb.nih.gov/ij/index.html (2009).